doi:10.1093/brain/aws041 Brain 2012: 135; 1017–1026 | 1017

BRAIN
A JOURNAL OF NEUROLOGY

Motor deficits correlate with resting state motor network connectivity in patients with brain tumours

Marc L. Otten,[1,*] Charles B. Mikell,[1,*] Brett E. Youngerman,[1] Conor Liston,[2] Michael B. Sisti,[1] Jeffrey N. Bruce,[1] Scott A. Small[3] and Guy M. McKhann, II[1]

1 Department of Neurological Surgery, Columbia University Medical Center, New York, NY 10032, USA
2 Department of Psychiatry, Neurology, and Neuroscience, Weill Medical College of Cornell University, New York, NY 10024, USA
3 Columbia University College of Physicians and Surgeons, Taub Institute for Research on Alzheimer's Disease and the Aging Brain, New York, NY 10032, USA

*These authors contributed equally to this work.

Correspondence to: Marc. L. Otten, MD,
Department of Neurosurgery,
Columbia University,
710 West 168th Street, Suite 4-404,
New York, NY 10032, USA
E-mail: mo2289@columbia.edu

While a tumour in or abutting primary motor cortex leads to motor weakness, how tumours elsewhere in the frontal or parietal lobes affect functional connectivity in a weak patient is less clear. We hypothesized that diminished functional connectivity in a distributed network of motor centres would correlate with motor weakness in subjects with brain masses. Furthermore, we hypothesized that interhemispheric connections would be most vulnerable to subtle disruptions in functional connectivity. We used task-free functional magnetic resonance imaging connectivity to probe motor networks in control subjects and patients with brain tumours ($n = 22$). Using a control dataset, we developed a method for automated detection of key nodes in the motor network, including the primary motor cortex, supplementary motor area, premotor area and superior parietal lobule, based on the anatomic location of the hand-motor knob in the primary motor cortex. We then calculated functional connectivity between motor network nodes in control subjects, as well as patients with and without brain masses. We used this information to construct weighted, undirected graphs, which were then compared to variables of interest, including performance on a motor task, the grooved pegboard. Strong connectivity was observed within the identified motor networks between all nodes bilaterally, and especially between the primary motor cortex and supplementary motor area. Reduced connectivity was observed in subjects with motor weakness versus subjects with normal strength ($P < 0.001$). This difference was driven mostly by decreases in interhemispheric connectivity between the primary motor cortices ($P < 0.05$) and between the left primary motor cortex and the right premotor area ($P < 0.05$), as well as other premotor area connections. In the subjects without motor weakness, however, performance on the grooved pegboard did not relate to interhemispheric connectivity, but rather was inversely correlated with connectivity between the left premotor area and left supplementary motor area, for both the left and the right hands ($P < 0.01$). Finally, two subjects who experienced severe weakness following surgery for their brain tumours were followed longitudinally, and the subject who recovered showed reconstitution of her motor network at follow-up. The subject who was persistently weak did not reconstitute his motor network. Motor weakness in subjects with brain tumours that

Received August 14, 2011. Revised January 4, 2012. Accepted January 23, 2012. Advance Access publication March 8, 2012

do not involve primary motor structures is associated with decreased connectivity within motor functional networks, particularly interhemispheric connections. Motor networks become weaker as the subjects become weaker, and may become strong again during motor recovery.

Keywords: resting-state functional MRI; brain tumour; resting-state; motor network; primary motor cortex; supplementary motor area; grooved pegboard

Abbreviations: PMA = premotor area; PMC = premotor cortex; SMA = supplementary motor area; SPL = superior parietal lobule

Introduction

Maximal resection and preservation of neurological function are key principles in surgery for brain tumours (Sanai and Berger, 2008; McGirt *et al*., 2009; Chaichana *et al*., 2011). However, functional localization in neurosurgery, by both imaging and neurophysiological techniques, has been hampered by an outmoded, localizationist model of brain function. It is now widely acknowledged that there is no 'language centre' or 'vision centre', but rather, these functions are distributed across vast, cortico-subcortical networks (Sporns, 2011). This has been termed the hodotopological model (De Benedictis and Duffau, 2011). As neurologists and neurosurgeons work in concert to preserve these large-scale networks during brain tumour surgeries, new tools for their identification are urgently needed. Task-free functional magnetic resonance connectivity (functional connectivity MRI) has provided a powerful tool for description and investigation of these networks (Biswal *et al*., 1995, 2010; Salvador *et al*., 2005). Recent demonstrations of tight correlation between neuroanatomical structure and functional networks observed with functional connectivity MRI (Margulies *et al*., 2009; Kelly *et al*., 2010) have supported the potential utility of this modality. However, further studies on the exact relationship between structural and functional connectivity are needed.

Voluntary motor action is supported by a network involving numerous brain structures, including the primary motor cortex, the premotor areas (PMA) [including the supplementary motor area (SMA)], and the superior parietal lobule (SPL). These structures are known to be activated in task-based functional MRI paradigms (Esterman *et al*., 2009; Post *et al*., 2009). These structures are all considered surgically 'eloquent' by classic definitions (Spetzler and Martin, 1986). However, avoidance of interruption of their connections has only begun to be considered in surgical planning (Sanai and Berger, 2010; Martino *et al*., 2011). It is very unusual for a brain mass to arise within one of these cortical structures; it is more typical for them to arise in subcortical white matter (Canoll and Goldman, 2008). How these white matter lesions, which do not directly impact eloquent tissue, cause motor weakness is not clear. This allows us to test the hypothesis that disruptions in functional connectivity lead to motor weakness in patients with brain tumours. Clear description of how functional connectivity deficits lead to motor weakness is needed to establish the use of resting functional MRI as a clinical tool for surgical planning.

Furthermore, we hypothesized that long-distance connection, especially between hemispheres, would be especially vulnerable to injury. These white matter connections are predicted to be sparse and metabolically expensive. This is in accordance with neuroanatomical data (Schuz *et al*., 2006) and theoretical considerations relating to the proposed 'small world' architecture of brain networks (Sporns and Kotter, 2004; Sporns, 2011). Specifically, the small world hypothesis suggests that most network connections need be within local network hubs, with sparse connections between distant hubs (Sporns, 2011). The influence of mass lesions on connectivity within the motor network represents a unique opportunity to test this hypothesis.

Since the original observation of cross-correlation between the time-series of the primary motor cortices (Biswal *et al*., 1995), functional connectivity MRI has proven to be a powerful research tool. Despite these widespread applications, a number of questions remain about the utility of functional connectivity MRI for clinical purposes. Correlations between functional connectivity MRI and neuropsychometric tests have been limited in patients with brain tumours (Zhang *et al*., 2009). Analysis of the data is complex, and clinicians are not currently trained to interpret it. It has no widely accepted clinical use, though it shows promise in identifying language lateralization (Liu *et al*., 2009), differentiating Alzheimer's disease from frontotemporal dementia (Zhou *et al*., 2010), predicting motor recovery after stroke (Carter *et al*., 2010), among many other applications, which have been the subject of multiple reviews (Greicius *et al*., 2004, 2007; Bluhm *et al*., 2007; Wang *et al*., 2007; Supekar *et al*., 2008; Anand *et al*., 2009; Hedden *et al*., 2009; Li *et al*., 2009). Straightforward techniques for interpreting functional connectivity MRI data for clinical use are urgently needed.

In the present article, we report a rapid technique for demonstration of motor networks in a control dataset provided in the 1000 Functional Connectomes project (Biswal *et al*., 2010). We then show that selective loss of connectivity in this network is correlated with the presence of motor weakness in subjects with brain tumours, and we propose that interhemispheric connections (such as that between the right- and left-hand motor regions) are related to the generation of motor weakness. We focused on motor function because of the relative ease of assessment in a basic history and clinical exam. We use our technique to probe brain circuits underlying performance on a neuropsychometric test, the grooved pegboard, a measure of fine motor control. Finally, we show that networks observable with our technique track injury and recovery following brain surgery.

Materials and methods

Subjects

Participants in this study were identified from the group of patients seen in consultation by the Department of Neurological Surgery at the Neurological Institute of New York and the New York-Presbyterian Hospital, Columbia campus. Patients over age 18 who were diagnosed with an intracranial mass lesion, scheduled to have an MRI on our scanner, were offered participation in the study.

A total of 22 adult, right-handed patients with intra-axial lesions, who underwent surgical biopsy or resection between August 2010 and May 2011, participated in the study (Table 1). Of this group, 16 patients presented without motor weakness, while six patients presented with weakness based on history and clinical exam. The age range of participants was 31–77 years. An informed consent process was used to explain potential risks, benefits and alternatives to the study, including not participating. All patients signed informed consent prior to participation, in accordance with guidelines and approval of the institutional review board at Columbia University Medical Centre. Demographic and clinical information are presented in Table 2. Approximate tumour volume was calculated as anteroposterior dimension × mediolateral dimension × craniocaudal dimension.

A control dataset of right-handed subjects was obtained from the 1000 Functional Connectomes database (Biswal *et al*., 2010). Within the larger database, the Oxford dataset was used, as the scanning parameters were the closest to our own (3 tesla magnet, repetition time = 2, slices = 34, timepoints = 175). They included 22 subjects (12 male, 10 female) age 20–35 years (average = 29.0 years, SD = 3.7 years).

Neuropsychometric evaluation

Preoperative imaging and surgery proceeded according to established standards of care. All patients underwent neurological exam and abbreviated neuropsychometric testing at the time of imaging. The neuropsychometric testing included the Grooved Pegboard test, a test of manual dexterity, which involves the motor network (Lafayette Instrument Company). The test was administered twice, to evaluate function of dominant and non-dominant hands. Clinical exam included a history, assessment of cranial nerve function, motor function in all extremities, sensory function, and deep tendon reflexes.

Image acquisition

In all subjects, task-free functional MRI was acquired on a 3.0 T magnetic resonance scanner with head coil supplied by the vendor

Table 1 Demographics, tumour type and surgical approach

	Age (years)	Gender	Tumour side	Lobe	Tumour type	Surgery
Asymptomatic	31.6	F	Right	Frontal/ Temporal	Tanycytic ependymoma (Grade II)	R frontotemporoparietal craniotomy, resection via transsylvian approach
	34.2	F	Left	Temporal	Diffuse astrocytoma (Grade II)	L temporal awake craniotomy
	36.0	F	Right	Frontal	Anaplastic astrocytoma (Grade III)	R frontal craniotomy, resection
	76.9	M	Left	Frontal	Diffuse large B cell lymphoma	L frontal craniotomy, biopsy/partial resection
	73.4	F	Bilateral	Cerebellum	Lung metastasis	Suboccipital craniotomy tumour decompression
	64.4	M	Left	Frontal/ Parietal	Lung metastasis	L frontoparietal craniotomy tumour
	39.7	M	Right	Temporal	Mixed glial-neuronal neoplasm with features of DNET/gangliocytoma (Grade I)	RFT craniotomy tumour
	54.4	M	Right	Temporal	Anaplastic astrocytoma (Grade III)	Stereotactic biopsy
	44.2	M	Right	Temporal	Glioblastoma multiforme (Grade IV)	R temporal craniotomy tumour
	57.7	F	Right	Temporal	Glioblastoma multiforme (Grade IV)	R craniotomy, cyst drainage and tumour debulking
	53.6	M	Bilateral	Corpus Callosum	Glioblastoma multiforme (Grade IV)	L frontal stereotactic biopsy
	52.0	M	Right	Occipital	Lymphoma	R occipital craniotomy, open biopsy
	35.8	F	Left	Occipital	Glioblastoma multiforme (Grade IV)	L occipital craniotomy, resection
	40.9	F	Right	Temporal	Astrogliosis and Chaslin's marginal gliosis/sclerosis	R temporal craniotomy, resection of R anterior temporal lobe including uncus and amygdala, sparing hippocampus
	59.0	M	Right	Temporal	Glioblastoma multiforme (Grade IV)	R temporal craniotomy, resection
	75.2	F	Left	Temporal	Anaplastic astrocytoma (Grade III)	L temporal craniotomy, radical subtotal resection
Symptomatic	35.7	M	Left	Frontal	Glioblastoma multiforme (Grade IV)	Awake craniotomy, cortical mapping and stimulation
	77.7	M	Right	Frontal	Lung metastasis	R rolandic awake craniotomy, resection
	61.2	M	Right	Frontal	Glioblastoma multiforme (Grade IV)	Bifrontal craniotomy, resection
	62.7	F	Right	Frontal	Glioblastoma multiforme (Grade IV)	R frontal craniotomy, resection
	55.1	M	Left	Temporal	Glioblastoma multiforme (Grade IV)	L temporal craniotomy, resection
	73.9	F	Right	Frontal	Breast metastasis	R frontal craniotomy, resection

F = female; L = left; M = male; R = right; T = temporal.

Table 2 Characteristics of full strength and weak subjects

	Full strength	Weak	*P*-value
n	16	6	
Female gender	7	2	0.66
Age	49.6	61.0	0.23
Volume (cc)	27	44	0.39
Pathology - high grade	12	6	0.18
Pathology - low grade	4	0	0.18
Right Hemisphere	9	4	0.66
Antiepileptic drugs	12	4	0.70
Steroids	8	6	0.03

(General Electric). Head movement was restricted using a pillow and foam, and earplugs were used to attenuate scanner noise and maximize patient comfort. During the functional runs, the participants were instructed to close their eyes. Participants were asked to stay awake and remain as still as possible. A total of 180 multi-slice T_2*-weighted functional MRI images were obtained with a gradient echo-planar sequence using axial slice orientation (27 slices, slice thickness = 5 mm, spacing = 0 mm, field of view = 21 cm^2, phase field of view 1.00 cm^2, frequency = 64 Hz, phase = 64, repetition time = 2000 ms, echo time- = 30 ms, flip angle = 90°). A T_1 magnetization prepared rapid gradient echo sequence was also acquired in the same session for co-registration with functional data.

Post-processing and data analysis

MRI data were pre-processed prior to performing a functional connectivity analysis. Pre-processing included spatial smoothing using a 5-mm full-width, half-maximum Gaussian kernel, slice scan time correction and 3D motion filtering. Temporal filtering was optimized for the functional connectivity analysis, which assesses correlations in low-frequency variation, as described in Biswal *et al*. (2010). Using publicly available scripts from the 1000 Functional Connectomes Project (Biswal *et al*., 2010), we stripped skull, segmented grey matter, white matter and CSF, and regressed out nuisance parameters. After pre-processing, corticocortical functional connectivity was assessed using a seed-based approach, according to methods described elsewhere (Fox *et al*., 2005; Biswal *et al*., 2010). In brief, the blood oxygen level-dependent signal time-courses for seed regions located in the right and left hand-motor knobs in the primary motor cortex were cross-correlated voxelwise on every other signal time-course in a whole brain analysis, while regressing out the effect of nuisance signals, and the regression coefficients were *Z*-transformed. This generated whole-brain functional connectivity maps for each subject representing the strength of correlated resting state blood oxygen level-dependent signal fluctuations for each seed volume. Co-registration was verified by inspection of key anatomic landmarks, including the ventricles, the corpus callosum and prominent sulci. All scans are available online at web addresses listed in Supplementary Table 1.

Anatomical localization of the supplementary motor area, premotor area and superior parietal lobule

Using the functional connectivity maps generated by cross-correlation with each hand-motor region, voxels of maximum cross-correlation were identified within frontal and parietal locations where the SMA, PMA and SPL are located. Because of anatomic displacement of motor structures secondary to tumour, maximal cross-correlation (between the left and right primary motor cortices, for each side, respectively) was used to identify the SMA, PMA and SPL. Coordinates in Talairach space are as follows: left PMC, [42–48; 33–39; 38–44]; left SMA, [38–44; 38–44; 31–35]; left PMA, [33–39; 45–51; 41–47]; left SPL, [39–45; 23–29; 40–46]; right PMC, [16–22; 32–38; 42–48]; right SMA, [23–29; 39–45; 39–45]; right PMA, [33–39; 45–51; 12–18]; right SPL, [39–45; 23–29; 15–21]. The voxel of maximum cross-correlation within the coordinate ranges was identified as the centroid of the SMA, PMA, SPL or PMC. The procedure was carried out twice, once for the right PMC and once for the left. Images were imported into the Python environment using PyNifti, and time-series analysis was carried out with the Nitime package (Millman and Brett, 2007; Hanke *et al*., 2009), as well as custom Python scripts. A matrix of cross-correlation between each time-series was then constructed by pairwise Pearson cross-correlation of the pre-processed data, resulting in an 8 × 8 matrix (e.g. left PMC-left PMC, left PMC-left SMA, etc.). These 'adjacency matrices' (Bullmore and Sporns, 2009) were used to create weighted, undirected graph representation of the motor network in Nitime. Mean functional connectivity was also calculated by calculating the mean of each connection within the adjacency matrix, while ignoring self connections (e.g. left PMC-left PMC). For the first figure, broadband coherence in the 0.08–0.15 Hz band was used to construct the adjacency matrix. Coherence was calculated between 0.02 and 0.15 Hz, intended to have a band-pass similar to the cross-correlation analysis. Using the Nitime package, the power of given frequency bands of interest was calculated using Welch's method and Fast Fourier Transforms. Coherence was calculated between derived bands in this spectrum, and averaged across all of the bands, which is reported as a quantity between 0 and 1. Graphs were plotted with the NetworkX (Hagberg, 2008) software in the Matplotlib environment.

Statistics

Statistical comparisons between groups were carried out by non-parametric tests. Mean functional connectivity was calculated as the mean edge weight among unique edges in the graph. When statistical comparisons were performed for individual connections, differences in mean edge weights were computed using the Mann–Whitney U test. Where Bonferroni correction is reported, the *P*-value reported has been multiplied by the number of tests, and the threshold for statistical significance remains 0.05.

Results

Interhemispheric functional connectivity in the motor network, lateralizing to the left

We applied our technique to a control dataset provided publicly as part of the 1000 Functional Connectomes project (Biswal *et al*., 2010, http://www.nitrc.org/projects/fcon_1000), and we calculated Pearson cross-correlation in the acquired data between the regions defined as PMC, SMA, PMA and SPL. Strong functional connectivity was observed between each of these regions (Fig. 1), supporting their connectivity in a motor network. Cross-correlation

was used to create a weighted, undirected graph representation of the motor network (Fig. 1B). Strong connectivity was observed between the primary motor cortices bilaterally, as well as between the SMAs. Connectivity was stronger with the left parietal lobule than the right, consistent with the known role of the dominant SPL in motor networks (Russell *et al*., 2005; Liu *et al*., 2009). Within subjects, weights of each edge were normally distributed around the mean weights. Age effects were not observed; there was no correlation between age and mean connectivity within networks (Pearson and Spearman correlations, P = not significant).

Patients with brain tumours but normal motor strength have motor networks qualitatively similar to controls

We performed the same analysis on 16 subjects with brain tumours but no motor weakness (Table 1). No lesions in this dataset directly affected the PMCs. The intrinsic architecture was similar, with strong interhemispheric functional connections between homologous structures (especially the SMAs and the PMCs) and marked connectivity to the dominant SPL (Fig. 2, *left*). Interestingly, mean connectivity in this dataset was much greater than in the control subjects (0.44 versus 0.33, $P < 0.00001$, Mann–Whitney U test).

Patients with motor weakness exhibit diminished functional connectivity within the canonical motor network, especially in interhemispheric connections

Subjects with motor weakness ($n = 6$) had diminished mean functional connectivity in the motor network, compared to non-weak subjects (0.44 versus 0.38, $P < 0.001$, Mann–Whitney U test) (Fig. 2, *centre*). Average network connectivity was also greater in this dataset than in the control dataset ($P < 0.001$, Mann–Whitney U test). The most consistently weakened connections were interhemispheric ones (Fig. 2, *right*): between the left PMC and the right PMA ($P < 0.01$, Mann–Whitney U test), the primary motor cortices, ($P < 0.05$), the left SMA and right PMA ($P < 0.05$), and the left SPL and right PMA ($P < 0.05$). No changes in intrahemispheric connections met statistical significance.

Performance on the grooved pegboard is lateralized to the dominant hemisphere

To assess subtle deficits in motor function in patients lacking overt weakness, we administered the grooved pegboard neuropsychological test to 12 enrolled subjects for both dominant and non-dominant hands. The subject was asked to place 25 pegs into holes on a board, moving from left to right with the right hand, and right to left with the left hand, and top to bottom, as quickly as possible. Performance for both dominant and non-dominant hands was tightly correlated to connectivity between the left PMA and left SMA (Fig. 3), ($R = 0.85$, $P < 0.05$ for dominant hand, Bonferroni corrected, $R = 0.92$, $P < 0.001$ for non-dominant hand, Bonferroni corrected). These relationships were robust to partial correlation with age as a covariate, even after Bonferroni correction ($P < 0.01$ for the non-dominant hand, $P < 0.05$ for the dominant hand). Connectivity between the left PMC and PMA correlated with performance on the pegboard for dominant and non-dominant hands ($R = 0.63$ and 0.77, respectively), though this did not survive correction for multiple comparisons. No similar correlation was seen in the right hemisphere between the PMA and SMA (Fig. 3, *bottom*). This led us to hypothesize that overall connectivity (e.g. its degree in the graph) of the left PMA would correlate with pegboard performance. Left PMA degree correlated with both dominant ($R = 0.63$) and non-dominant ($R = 0.61$) performance on the pegboard (Fig. 4). This relationship was strengthened by partial correlation with age as a covariate ($P < 0.01$ for both). This suggests a role for circuitry connected to the dominant PMA for pegboard performance.

Motor network integrity correlates with postoperative motor weakness and long-term functional recovery

Five subjects were followed with serial scans following their initial surgery. Two subjects emerged from the initial surgery profoundly weak, and both gradually recovered function (Fig. 4). Subject 42 recovered from near-hemiparesis on the first postoperative day, to full strength (5/5 to confrontational testing), by the follow-up scan at 5 months. Subject 42 underwent resting-state functional MRI prior to surgery, on the first postoperative day, and at 5 months. Mean connectivity strength was significantly different across the three scans (Fig. 4A–D) (0.47 for the initial scan, 0.05 for the immediate postoperative scan and 0.62 at follow-up; $P < 0.0001$, Kruskal–Wallis test). By contrast, a nearly age-matched control, Subject 27 (34 versus 36 years old), who did not experience postoperative motor weakness, did not have significantly different mean connection strength between her initial, postoperative and follow-up scans (Fig. 4E–H, 0.13, 0.22 and 0.29, P = not significant). Subject 28 had significant weakness preoperatively, which acutely worsened postoperatively, and did not fully recover by follow-up; his motor networks remained relatively weak (Fig. 4I–L, 0.15, 0.08 and 0.07), and did not significantly change. Of note, one subject who fully recovered motor strength had de-correlated motor networks at follow-up. In all other cases, the motor networks strengthened over time.

Discussion

In the present manuscript we report that motor networks in subjects with brain tumours are comparable to those observable in control patients, and that left frontal connections between the PMA and SMAs are critical for motor performance. We show

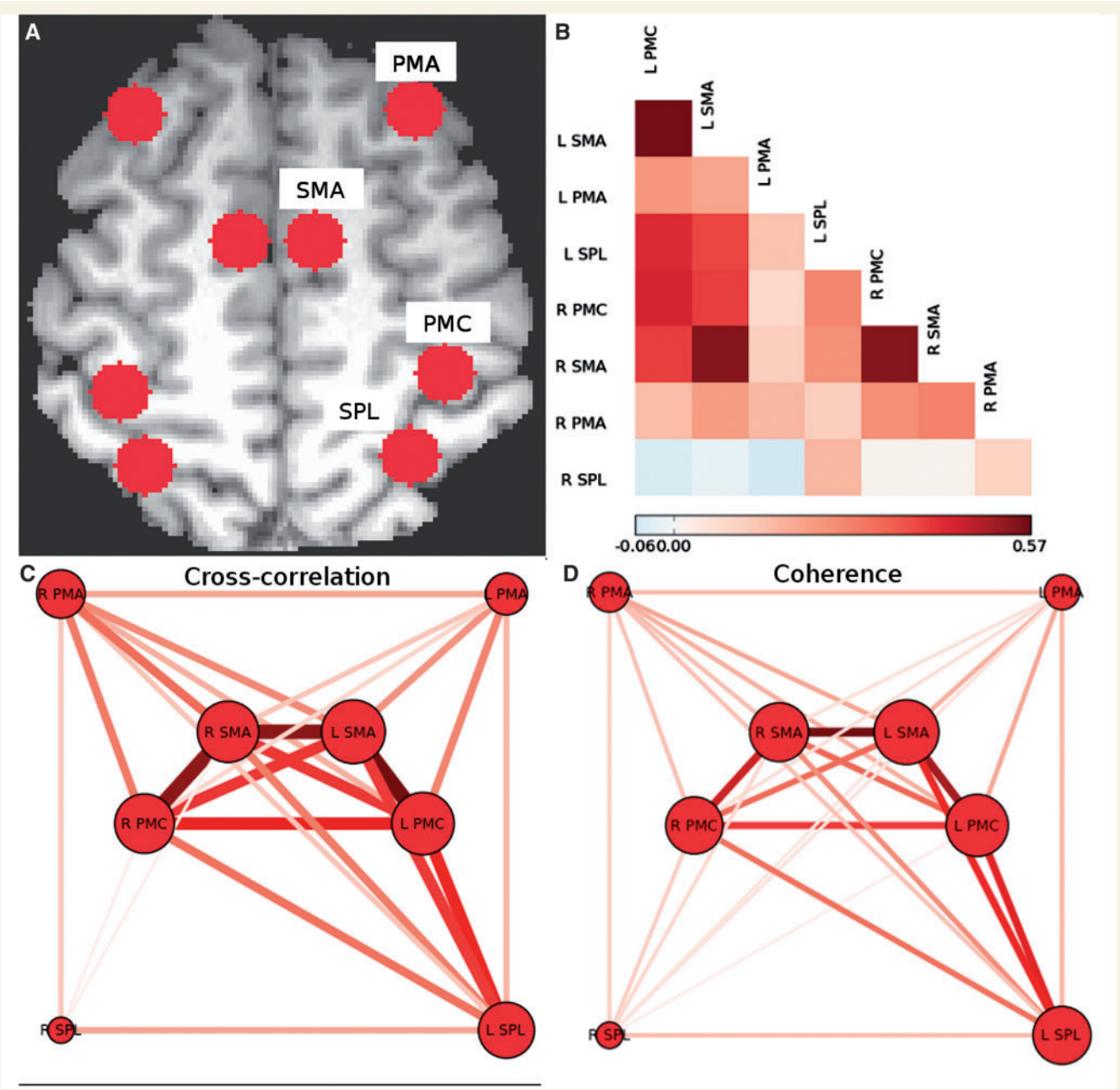

Figure 1 Motor networks in control subjects. (**A**) Single voxels identified as centroids of regions corresponding to PMC, SMA, PMA and SPL were identified in each hemisphere bilaterally. (**B**) Pairwise Pearson cross-correlation was calculated between each region, and adjacency matrices were constructed. Scale bar, Pearson correlation (0.06–0.57). (**C**) Weighted, undirected graphs were constructed from adjacency matrices derived from cross-correlations. Strong cross-correlation was observed within each hemisphere and across hemispheres between homologous structures. This representation is an average of the 22 subjects in our control dataset. (**D**) Coherence in the 0.08–0.15 Hz band was used to construct adjacency matrices, which showed similar architecture to graphs derived from cross-correlation. L = left; R = right.

that patients who presented with motor weakness have significantly decreased mean motor network connectivity. Finally, we found two patients who became acutely weak after surgery and show that recovery tracks motor network connectivity. We developed a computationally simple, straightforward method of demonstrating the anatomic location of nodes corresponding to SMA, PMA and SPL, when the location of the motor cortex is known. A drawback of our approach is that it requires registration to a standard brain, but it is possible that this step could be avoided in some circumstances. Nonetheless, our technique is suitable for rapid translation to clinical use.

There are several caveats to the interpretation of our data. Jiang *et al.* (2010) report that brain lesions, especially high-grade gliomas in the primary motor cortex, dampen or limit task-based

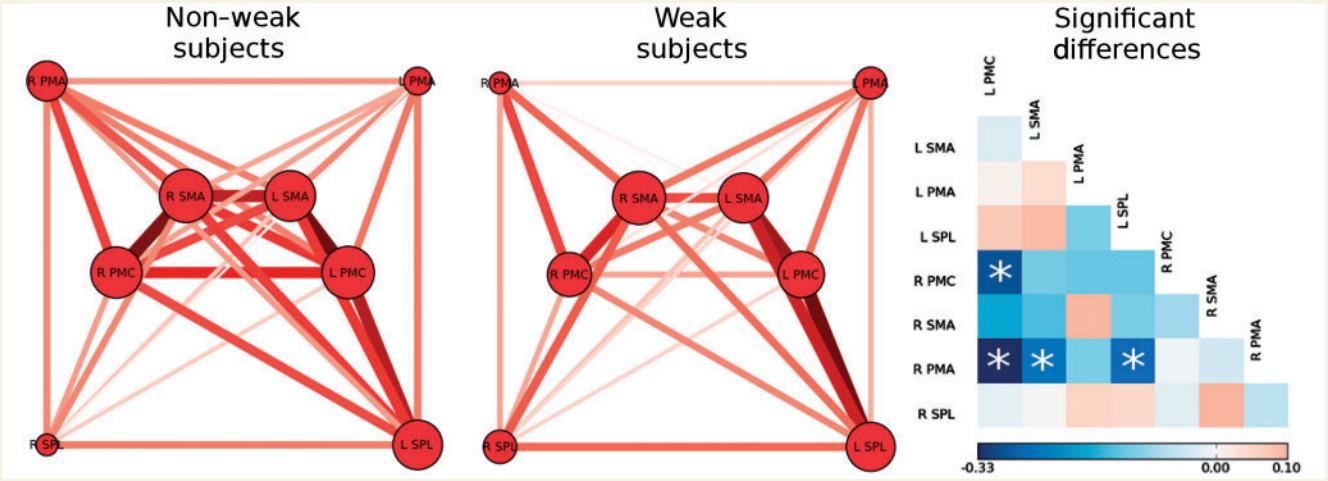

Figure 2 Weak subjects have significantly weaker mean connectivity than control subjects. *Left*: The overall structure of the motor network in patients with brain tumours is similar to that of controls. Connectivity is most pronounced between the SMAs, PMCs and the dominant SPL. *Middle*: Subjects with motor weakness largely preserve intrahemispheric connectivity, but interhemispheric connections are significantly weaker. *Right*: The largest differences in connectivity between weak and non-weak subjects were between the left PMC and right PMA, the left and right PMCs, the right PMA and left SMA, and the right PMA and left SPL. Scale bar, Pearson correlation. $^{*}P < 0.05$.

blood oxygen level-dependent oscillations. Our data suggest, however, that cross-correlation between resting oscillations in motor structures is robust to the presence of lesions, even high-grade ones (Fig. 4). We also acknowledge that functional zones can move in the presence of neoplastic disease, especially with low-grade lesions (Duffau *et al*., 2003). By identifying the areas of maximum cross-correlation, our technique is robust to a certain amount of functional translocation. We do acknowledge that it is possible that motor areas have translocated outside of the margins allowed by the voxel requirement. In our series, however, the main motor networks appear to be similar in spatial architecture between patients and controls.

Our demonstration that motor networks are similar between patients with brain tumours and controls illustrates several points. The finding of higher average connectivity in patients with brain tumours versus controls suggests that the brain adapts to lesion growth by distributing functions across networks, increasing, rather than decreasing, connectivity. While this finding must be interpreted with caution, given different scan parameters and subject demographics, heightened connectivity in this population is consistent with adaptive functional reorganization. Furthermore, the failure of interhemispheric connections in weak patients supports bilateralization and distribution of function across hemispheres when a lesion appears. This is consistent with the interpretation that failure of distribution across hemispheres leads to motor weakness.

Our data suggest that motor performance, as measured by the grooved pegboard exam, is not bilateral, but localized to the left frontal lobe, especially the left PMA. To date, no study has directly examined the circuits that support performance on the grooved pegboard. Other reports have suggested that subclinical frontal ischaemia may worsen pegboard performance (Wright *et al*., 2008), and that frontal white matter atrophy correlates to pegboard performance in healthy older adults (Kochunov *et al*., 2010). We extend these findings by implicating specific structures in performance.

Motor recovery after brain injury is a distributed process, and our data suggest that networks return to preoperative conditions as strength returns. Of note, in the subject who returned to full strength after 5 months, her average connectivity exceeded preoperative connectivity. This suggests that the healing process involves distribution of function to other areas of the network, including the contralateral hemisphere. Rehabilitative strategies boosting contralesional function may, therefore, improve outcomes. This also supports recent reports (Jang, 2011) that the contralesional primary motor cortex is involved in post-stroke recovery. The determination of anatomical locations for SMA, PMA and SPL based on resting-state data leads to the possibility that this information might be utilized to construct preoperative maps to determine whether these structures should be avoided surgically. This information could be integrated with available neuro-navigational systems to delimit the boundaries of 'functional tissue', extending beyond traditional methods that only identify the primary motor area. Our techniques have the potential to both advance understanding of motor systems physiology and function, and to improve patient outcomes following brain tumour surgery.

Conclusion

Motor networks in patients with brain tumours are demonstrable using functional connectivity MRI. These networks are different in subjects with and without motor weakness, and predict motor performance. Further work will be required to use these networks to predict surgical risk and potential rehabilitative outcome.

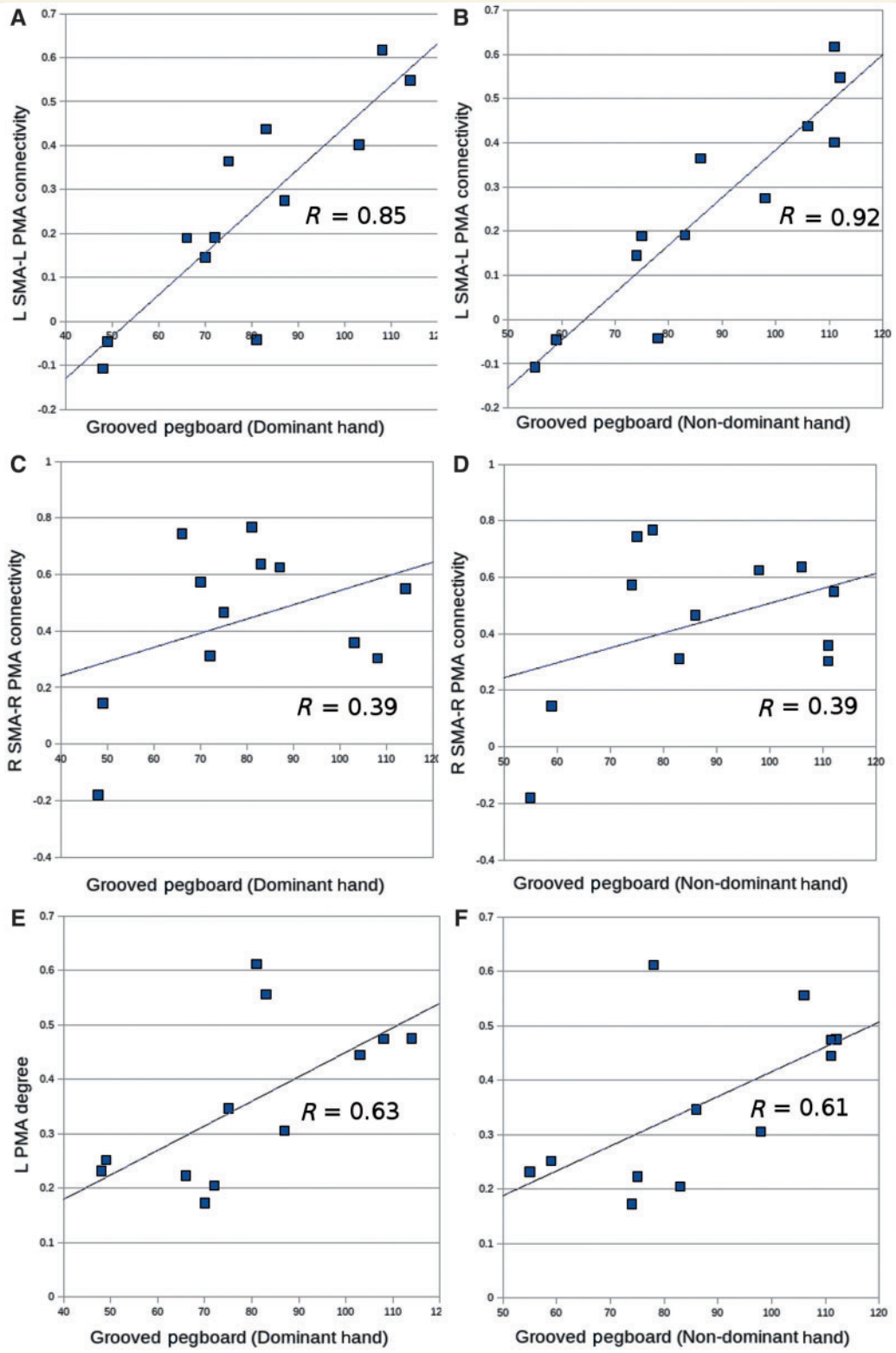

Figure 3 (**A** and **B**) Strong correlation is observed between left SMA–left PMA connectivity and performance on the grooved pegboard, with both the dominant and non-dominant hands ($P < 0.001$ for both, Bonferroni corrected). (**C** and **D**) Non-significant correlation is seen between the right SMA–right PMA for both the dominant and non-dominant hands. (**E** and **F**) Left PMA degree correlated with pegboard performance with the dominant and non-dominant hands in a linear (Pearson) fashion ($P = 0.03$ and $P = 0.03$, respectively). This sample excludes patients with weakness on gross motor testing. L = left; R = right.

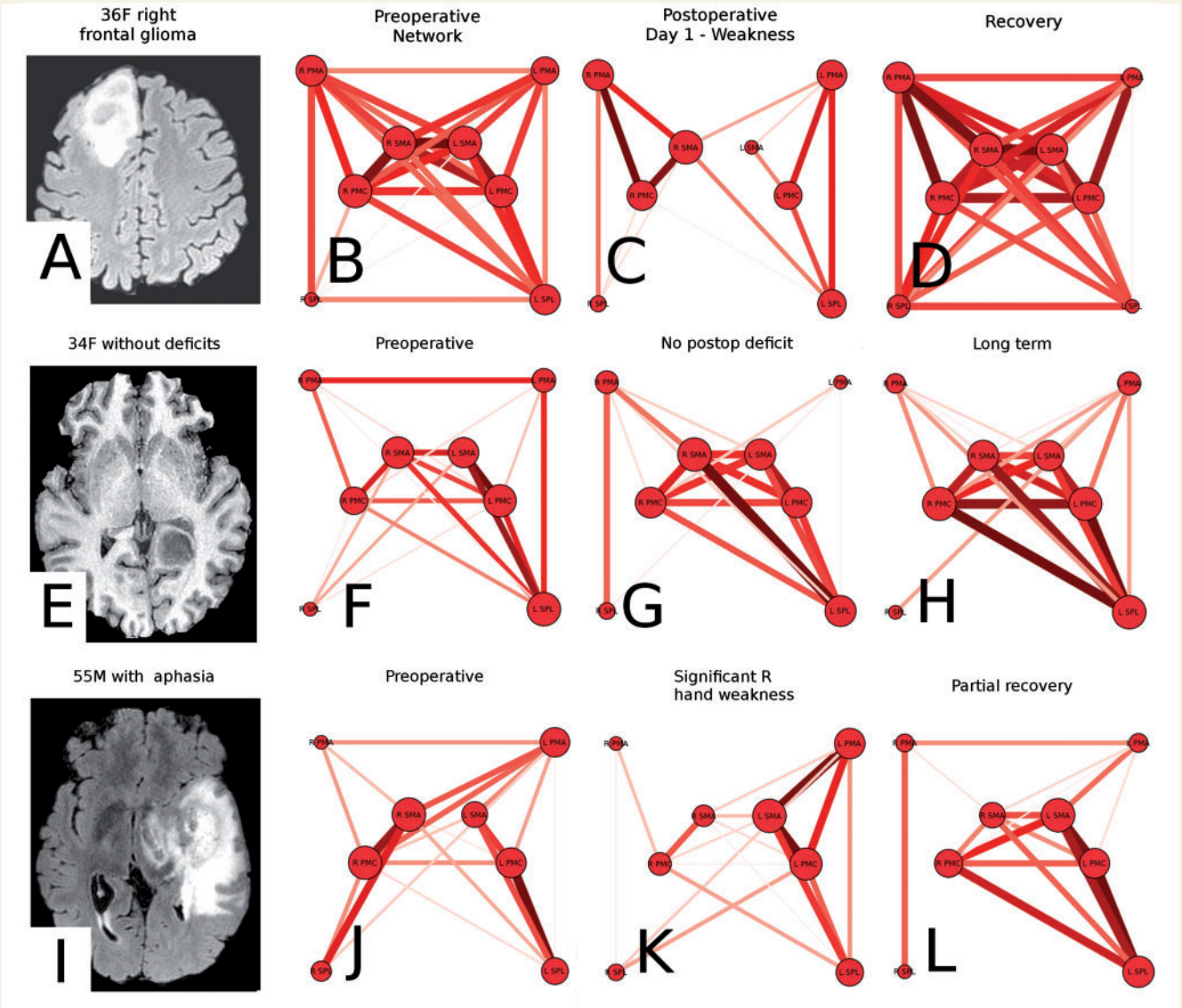

Figure 4 (**A**) A 36-year-old female presented with a single seizure and was found to have a large right frontal mass. The mass displayed wispy contrast enhancement consistent with an anaplastic astrocytoma. The mass was very close to areas likely serving as the right-sided SMA. Following surgery, she was profoundly weak on her left side, unable to lift her left hand or arm off the bed. (**B**) Her preoperative motor network had strong connectivity between all nodes. (**C**) Interrogation of her motor network following injury showed markedly decreased connectivity throughout. (**D**) After recovery to nearly full strength, 5 months later, her motor networks strongly recovered as well. (**E**) Subject 27 had no clear preoperative deficits. Her preoperative T_1-weighted MRI. (**F**) Her motor network qualitatively resembles control networks. (**G**) Her immediate postoperative motor network is similar. (**H**) At long-term follow-up, her network resembles control networks. (**I**) Subject 28 had a right temporal glioblastoma, and presented with language difficulties, as well as a left-sided pronator drift. (**J**) His preoperative network is significant for weakened interhemispheric connections. (**K**) He was profoundly weak postoperatively. (**L**) At 3-month follow-up, his clinical and network strength had only partially recovered.

Supplementary material

Supplementary material is available at *Brain* online.

Acknowledgements

The authors would like to acknowledge L. DeLaPaz, F. Osorio, J. Thompson and T. Wojtasiewicz for their contributions to data acquisition and analysis; M.A. Siefring and T.F. Smusz for subject recruitment; and S.M. Smith, C.E. Mackay, and colleagues at the University of Oxford for contributing their data to the 1000 Functional Connectomes project.

Funding

Funding from within the department of Neurosurgery.

References

Anand A, Li Y, Wang Y, Lowe MJ, Dzemidzic M. Resting state corticolimbic connectivity abnormalities in unmedicated bipolar disorder and unipolar depression. Psychiatry Res 2009; 171: 189–98.

Biswal B, Yetkin FZ, Haughton VM, Hyde JS. Functional connectivity in the motor cortex of resting human brain using echo-planar MRI. Magn Reson Med 1995; 34: 537–41.

Biswal BB, Mennes M, Zuo XN, Gohel S, Kelly C, Smith SM, et al. Toward discovery science of human brain function. Proc Natl Acad Sci USA 2010; 107: 4734–9.

Bluhm RL, Miller J, Lanius RA, Osuch EA, Boksman K, et al. Spontaneous low-frequency fluctuations in the BOLD signal in schizophrenic patients: anomalies in the default network. Schizophr Bull 2007; 33: 1004–12.

Bullmore E, Sporns O. Complex brain networks: graph theoretical analysis of structural and functional systems. Nat Rev Neurosci 2009; 10: 186–98.

Canoll P, Goldman JE. The interface between glial progenitors and gliomas. Acta Neuropathologica 2008; 116: 465–77.

Carter AR, Astafiev SV, Lang CE, Connor LT, Rengachary J, Strube MJ, et al. Resting interhemispheric functional magnetic resonance imaging connectivity predicts performance after stroke. Ann Neurol 2010; 67: 365–75.

Chaichana KL, Halthore AN, Parker SL, Olivi A, Weingart JD, Brem H, et al. Factors involved in maintaining prolonged functional independence following supratentorial glioblastoma resection. Clinical article. J Neurosurg 2011; 114: 604–12.

De Benedictis A, Duffau H. Brain hodotopy: from the esoteric concept to the practical surgical applications. Neurosurgery 2011; 68: 1709–23.

Duffau H, Capelle L, Denvil D, Sichez N, Gatignol P, Lopes M, et al. Functional recovery after surgical resection of low grade gliomas in eloquent brain: hypothesis of brain compensation. J Neurol Neurosurg Psychiatry 2003; 74: 901–7.

Esterman M, Chiu YC, Tamber-Rosenau BJ, Yantis S. Decoding cognitive control in human parietal cortex. Proc Natl Acad Sci USA 2009; 106: 17974–9.

Fox MD, Snyder AZ, Vincent JL, Corbetta M, Van Essen DC, Raichle ME. The human brain is intrinsically organized into dynamic, anticorrelated functional networks. Proc Natl Acad Sci USA 2005; 102: 9673–8.

Greicius MD, Srivastava G, Reiss AL, Menon V. Default-mode network activity distinguishes Alzheimer's disease from healthy aging: evidence from functional MRI. Proc Natl Acad Sci USA 2004; 101: 4637–42.

Greicius MD, Flores BH, Menon V, Glover GH, Solvason HB, Kenna H, et al. Resting-state functional connectivity in major depression: abnormally increased contributions from subgenual cingulate cortex and thalamus. Biol Psychiatry 2007; 62: 429–37.

Hanke M, Halchenko YO, Sederberg PB, Hanson SJ, Haxby JV, Pollmann S. PyMVPA: a python toolbox for multivariate pattern analysis of fMRI data. Neuroinformatics 2009; 7: 37–53.

Hedden T, Van Dijk KR, Becker JA, Mehta A, Sperling RA, Johnson KA, et al. Disruption of functional connectivity in clinically normal older adults harboring amyloid burden. J Neurosci 2009; 29: 12686–94.

Jang SH. Contra-lesional somatosensory cortex activity and somatosensory recovery in two stroke patients. J Rehabil Med 2011; 43: 268–70.

Jiang Z, Krainik A, David O, Salon C, Tropres I, Hoffmann D, et al. Impaired fMRI activation in patients with primary brain tumors. Neuroimage 2010; 52: 538–48.

Kelly C, Uddin LQ, Shehzad Z, Margulies DS, Castellanos FX, Milham MP, et al. Broca's region: linking human brain functional connectivity data and non-human primate tracing anatomy studies. Eur J Neurosci 2010; 32: 383–98.

Kochunov P, Coyle T, Lancaster J, Robin DA, Hardies J, Kochunov V, et al. Processing speed is correlated with cerebral health markers in the frontal lobes as quantified by neuroimaging. Neuroimage 2010; 49: 1190–9.

Li Z, Moore AB, Tyner C, Hu X. Asymmetric connectivity reduction and its relationship to "HAROLD" in aging brain. Brain Res 2009; 1295: 149–58.

Liu H, Stufflebeam SM, Sepulcre J, Hedden T, Buckner RL. Evidence from intrinsic activity that asymmetry of the human brain is controlled by multiple factors. Proc Natl Acad Sci USA 2009; 106: 20499–503.

Margulies DS, Vincent JL, Kelly C, Lohmann G, Uddin LQ, Biswal BB, et al. Precuneus shares intrinsic functional architecture in humans and monkeys. Proc Natl Acad Sci USA 2009; 106: 20069–74.

Martino J, Honma SM, Findlay AM, Guggisberg AG, Owen JP, Kirsch HE, et al. Resting functional connectivity in patients with brain tumors in eloquent areas. Ann Neurol 2011; 69: 521–32.

McGirt MJ, Mukherjee D, Chaichana KL, Than KD, Weingart JD, Quinones-Hinojosa A. Association of surgically acquired motor and language deficits on overall survival after resection of glioblastoma multiforme. Neurosurgery 2009; 65: 463–9. discussion 469–70.

Millman KJ, Brett M. Analysis of functional magnetic resonance imaging in Python. Comput Sci Engineering 2007; 9: 52–55.

Post M, Steens A, Renken R, Maurits NM, Zijdewind I. Voluntary activation and cortical activity during a sustained maximal contraction: an fMRI study. Hum Brain Mapp 2009; 30: 1014–27.

Russell SM, Elliott R, Forshaw D, Kelly PJ, Golfinos JG. Resection of parietal lobe gliomas: incidence and evolution of neurological deficits in 28 consecutive patients correlated to the location and morphological characteristics of the tumor. J Neurosurg 2005; 103: 1010–7.

Salvador R, Suckling J, Coleman MR, Pickard JD, Menon D, Bullmore E. Neurophysiological architecture of functional magnetic resonance images of human brain. Cereb Cortex 2005; 15: 1332–42.

Sanai N, Berger MS. Glioma extent of resection and its impact on patient outcome. Neurosurgery 2008; 62: 753–64. discussion 264–6.

Sanai N, Berger MS. Intraoperative stimulation techniques for functional pathway preservation and glioma resection. Neurosurgical focus 2010; 28: E1.

Schuz A, Chaimow D, Liewald D, Dortenman M. Quantitative aspects of corticocortical connections: a tracer study in the mouse. Cerebral cortex 2006; 16: 1474–86.

Spetzler RF, Martin NA. A proposed grading system for arteriovenous malformations. Journal of neurosurgery 1986; 65: 476–83.

Sporns O, Kotter R. Motifs in brain networks. PLoS Biol 2004; 2: e369.

Sporns O. Networks of the brain. Cambridge: Mass; MIT Press; 2011.

Supekar K, Menon V, Rubin D, Musen M, Greicius MD. Network analysis of intrinsic functional brain connectivity in Alzheimer's disease. PLoS Comput Biol 2008; 4: e1000100.

Wang K, Liang M, Wang L, Tian L, Zhang X, Li K, et al. Altered functional connectivity in early Alzheimer's disease: a resting-state fMRI study. Hum Brain Mapp 2007; 28: 967–78.

Wright AA, Ranmuthugala G, Jones J, Maydom B, Disler P. Rural organisation of acute stroke teams project. Intern Med J 2008; 38: 32–7.

Zhang D, Johnston JM, Fox MD, Leuthardt EC, Grubb RL, Chicoine MR, et al. Preoperative sensorimotor mapping in brain tumor patients using spontaneous fluctuations in neuronal activity imaged with functional magnetic resonance imaging: initial experience. Neurosurgery 2009; 65: 226–36.

Zhou J, Greicius MD, Gennatas ED, Growdon ME, Jang JY, Rabinovici GD, et al. Divergent network connectivity changes in behavioural variant frontotemporal dementia and Alzheimer's disease. Brain 2010; 133: 1352–67.